# Photometric patterns as a key for determining the orientation of the rotation axis of RSO

**O.M. Kozhukhov**
*National Space Facilities Control and Test Center, Kyiv, Ukraine*
**N.I. Koshkin, L.S. Shakun**
*Astronomical Observatory of Odessa I.I. Mechnikov National University, Odessa, Ukraine*
**O.B. Bryukhovetskyi, O. Vasyltsiun**
*National Space Facilities Control and Test Center, Kyiv, Ukraine*
**T. Schildknecht, A. Vananti, P. Patole**
*Astronomical Institute, University of Bern, Bern, Switzerland*
**F. Piergentili, L. Mariani**
*University of Rome – La Sapienza, Rome, Italy*
**A. Hammet**
*UK Space Agency, Swindon, United Kingdom*
**R. Sherwood**
*NERC Space Geodesy Facility, Hailsham, United Kingdom*
**T. Yanagisawa, H. Kurosaki**
*Japan Aerospace Exploration Agency, Chofu, Tokyo, Japan*
**V. Kudak, V. Perig**
*Laboratory of Space Research of Uzhhorod National University, Uzhhorod, Ukraine*
**I. Salnikov, Y. Vovchyk**
*Astronomical Observatory of Lviv University, Lviv, Ukraine*
**I. Eglitis, J. del Pino, K. Salmins**
*Institute of Astronomy University of Latvia, Riga, Latvia*
**G. Bianchi**
*Italian National Institute for Astrophysics, Medicina, Italy*
**P. Di Lizia**
*Politecnico di Milano, Milan, Italy*

## ABSTRACT

Determining the rotation state of non-cooperative space objects is one of the tasks of the SSA. Estimation of their rotation rate and the spatial orientation of the rotation axis is necessary to predict their attitude, which is of great importance for both the success of active large space debris removal (ADR) missions and the improved propagation of RSO orbits on LEO. Monitoring the state of RSO can be carried out by various means, including using ground-based optical sensors by collecting photometric data, processing it and analyzing light curves. This paper discusses a technique for estimating the orientation of the RSO rotation axis in space, which is based on a structural analysis of RSO light curves and the search for similar fragments ("photometric patterns") in observations obtained from one or several sites synchronously, or sequentially over a short period of time. This approach does not assume knowledge of the body shape, so we use it to estimate the orientation of the rotation axis of two different RSOs, for one of which the shape information is completely missing. Photometric observations were obtained as part of two international campaigns: 87074G (R/B SL-14) was observed in 2020-2022 as part of the activities of the IADC, and observations of 82092A (COSMOS 1408; destroyed as a result of the use of an ASAT weapon on November 15, 2021) were acquired in 2023 - 2024 by observatories in Ukraine and some countries. The results of estimating the value and evolution of the rotation period, as well as the orientation of the rotation axis of RSO data, were obtained for time intervals with the highest density of observation series, are presented.

## 1. INTRODUCTION

Determining the rotation state of non-interacting space objects is one of the important tasks of SSA [1], [2]. Determining the spatial orientation of the spacecraft rotation axis is necessary to predict their position, which is of great importance both for the success of active debris removal (ADR) missions and for improving the propagation of RSO orbits on LEO. The most common method of monitoring the state of RSOs is by means of ground-based optical sensors with collecting photometric data, processing them, and analyzing obtained light curves (LC).

## 2. THEORETICAL BASIS OF THE "PHOTOMETRICAL PATTERNS" TECHNIQUE

This study will consider the application of a new method for analyzing a set of observed RSO LCs, proposed in [3], in order to determine the orientation of the satellite's rotation axis in space. This method is based on the structural analysis of LCs and the identification of a set of time moments at which light is reflected from the same areas of the spacecraft surface, i.e. located at the same latitude relative to the rotation axis. The novelty of the method is that no other information is used to obtain a solution, except the hypothesis of the equality of the normals' latitude of the light-reflecting surfaces at the corresponding moments in time (for example, not required information about the longitudinal location of the reflecting elements, and especially about the shape of the body). Also, precise measurement of the observation time is not required, and in some cases, high frequency and accuracy of brightness measurements are not required too.

We will consider the observed LCs of rotating RSOs, usually obtained over a large arc in the tracking mode [4]. It is known that many rotating RSOs make a full revolution around the center of mass in a fairly short time (~10-20 seconds). The man-made surface of these objects often consists of smooth areas with a high coefficient of specular reflection of light in the optical band. As a result, the LC often contains short-term bright outbursts of brightness, which are called "specular" flares for short [2]. This property of the LCs of some RSOs can be used to determine their rotation parameters using the above-mentioned method. For any moment in time, including the moment of observing any specular flare at a given site, we can calculate the coordinates of the phase angle bisector (PAB) vector in the inertial coordinate system (ICS). The PAB vector is necessary for the analysis of specular flares of brightness because such flare itself, according to the law of geometric optics, occurs only when some normal to the smooth surface of the satellite (flat, conical or cylindrical) coincides in direction with the PAB vector. During the rotation of the spacecraft, such a normal can approach the PAB vector once per revolution, which will be accompanied by a specular reflection of light towards the observer and the registration of a short-term flare of brightness. Thus, by calculating the position of the PAB vector at the moment of a flash of brightness, we thereby fix in the ICS the orientation of the normal to some area of RSO surface reflecting solar light (we fix the angles $\alpha$ and $\delta$).

Let us assume that the direction of the RSO rotation axis in the ICS changes slowly and during several orbital revolutions it can be considered fixed in space. Then in a non-rotating coordinate system, where the Z axis coincides with this spacecraft rotation axis (ARF – axis related frame), the direction of the PAB under consideration and the corresponding normal is specified by two other angles – longitude ($\lambda$) and latitude ($\beta$). On the other hand, these same light-reflecting surface areas and their normals have a fixed location on the spacecraft body and, if the rotation axis in the body is also fixed, then the normals have an invariable location in the rotating body fixed frame (BFF), namely, they have a fixed latitude angle ($\Phi$). Hence, for this specular flare of brightness we have the following equality $\Phi_i = \beta\_PAB_i$, which will be useful for solving the problem.

In [3], the concept of a "photometric pattern" was introduced. If two short sections of different LCs of a certain RSO contain the same characteristic pattern of brightness changes, then such a pattern can be called a repeating "photometric pattern". In the case of specular reflection of light, each original pattern ("recognizable" series of specular flares) can be determined by unique intervals between several RSO brightness flares on the interval of the rotation period (i.e., unique phase differences of these flares). In any case, only the current value of the slowly changing latitude $\beta$ of the PAB vector is important for the formation of a specular photometric pattern. Consequently, when the same values of the latitude of the corresponding PAB are realized for several different sensors (at completely different moments in time), then during the RSO's revolution, specular flares will occur from the same set of smooth edges on the spacecraft's body, and similar photometric patterns should be recorded on all LCs obtained by these sensors.

When analyzing LCs formed by mixed diffuse-specular reflection of light, it can be assumed that the same shape of patterns on different LCs is formed by successive reflection and diffuse scattering from the same set of illuminated and visible surface features. In the case of mixed reflection of light by a body with complex shape, the original pattern can be described as a characteristic combination of the shape and amplitude of a small section of the LC. With rapid rotation of the RSO, the pattern can most often be distinguished on the interval of one revolution of the RSO, but in the general case it can be formed on an interval shorter than the rotation period. In any case, this pattern can be associated with the average time of its appearance on the LC and the PAB coordinates in the ICS can be calculated for this moment.

Currently, identifying several patterns of different shapes in the structure of a LC and searching for similar patterns on another LC is a task for expert analysis. We hope that this procedure can be automated in the future, for example, by using artificial intelligence methods.

Thus, having identified several similar patterns in two or more RSO passes, we can assume (with varying degrees of confidence) that at the corresponding moments the sunlight is reflected from the same structural details on its surface. For any combination of specular flares in a pattern, the latitude of the corresponding normals in BFF should be very

close to the latitude of PAB in ARF at that moment. Let us assume that with mixed diffuse-specular reflection, each unique pattern can also be associated with the corresponding latitude of the PAB vector in ARF, as a characteristic of the "average" latitude of the normals of the light-reflecting areas on the spacecraft surface.

In the ideal case of essentially non-collinear directions of the PAB vectors, using their coordinates at average moments, even for two pairs of identical specular patterns, the position of the rotation axis in the ICS is determined confidently [3]. Then, the latitudes of the normals to the faces on the surface of the RSO can be found for the entire set of selected patterns.

However, for "conditionally identical" patterns of the mixed diffuse-specular type, the position of the rotation axis and, with it the average latitude of the set of surface elements forming this pattern, can be determined only with significant uncertainty. This is due to the fact that the pattern appearance in this case is influenced to varying degrees by inevitable differences in the current value of the phase angle and differences in the orientation of the scattering plane (plane: "Sun-RSO-observer") in different passes of this RSO. The accuracy of the solution for the rotation pole in this case depends on many factors, including the number of LCs used that demonstrate sufficiently similar patterns (type), the number of these patterns (types), the RSO trajectory and the geometry of its illumination and visibility from different sensors. Nevertheless, according to our assumption, for a RSO of arbitrary non-convex shape (often having smooth surface areas), it is the latitude angle of the PAB ($\beta$) that primarily determines the shape of the diffuse-specular pattern. Other geometric factors distort this pattern to varying degrees. The extent of this distortion cannot be theoretically estimated, since it is largely determined by the specific shape of the observed body. However, with a sufficient number of observations, the influence of these factors should average out, which may allow us to obtain a stable solution for the position of the rotation pole with a varying degree of uncertainty.

The mutual arrangement of the vectors defining the "observation geometry" relative to the axis of rotation of the RSO is shown on Fig. 1. In this figure, for the estimated position of the rotation pole $\Omega$, it is assumed that the arc "Sun-$\Omega$" has a fixed length according to the problem condition, and for the arcs "$PAB_n$-$\Omega$" (co-latitude $\beta'_n$ of the vector $PAB_n$) we also assume an unknown but identical length if the reflection of light in all cases occurs during the observability of identical patterns for different RSO-centric directions to the observer ($Obs_n$).
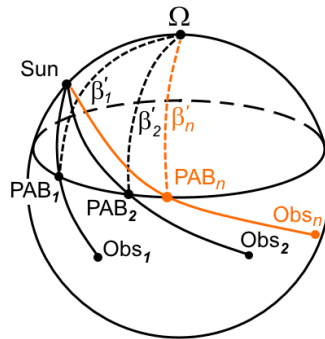


Fig. 1. Relative position of the rotation pole and vectors defining the RSO illumination and visibility geometry for n moments of time and the corresponding satellite-centric vectors of observers. Between PAB and the rotation axis the angle $\beta' = \pi/2 - \beta$.

## 3. OBSERVED OBJECTS

### 3.1 SL-14 R/B

One of the 3rd stages of the Tsiklon-3 rocket with USSPACECOM ID 18340 was included in the list of targets for rocket body photometry in accordance in the frames of IADC AI38.2. in 2020. Fig. 2 shows the time distribution of photometric observations of SC 18340 obtained in 2020-2022 at different observatories.
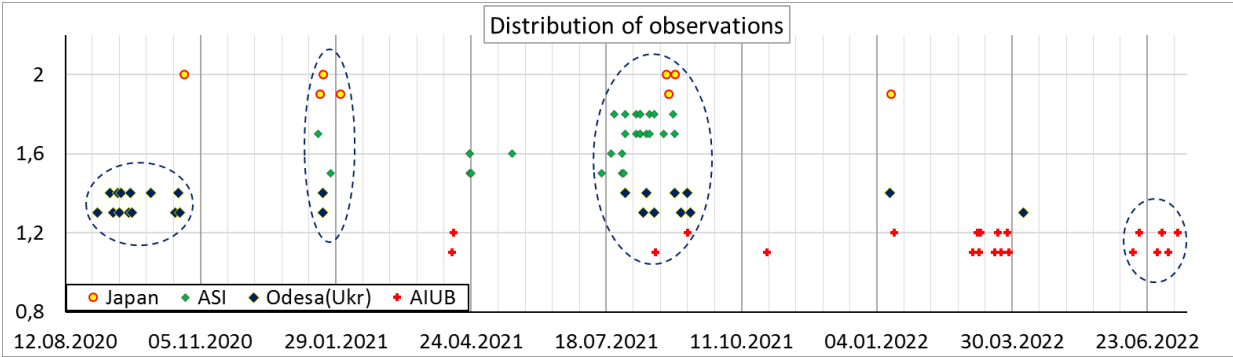
Fig. 2. Time distribution of 18340 photometric observations obtained in 2020-2022.

### 3.2 COSMOS 1408

On November 15, 2021, the Cosmos-1408 spacecraft (USSPACECOM ID 13552) was attacked by a Russian anti-satellite weapon. Numerous fragments were formed in orbit. German colleagues observed the fragments of destruction using the TIRA tracking and imaging radar. They came to the conclusion that the largest fragment is a partially preserved body of the spacecraft, and it is rotating rapidly [5]. They were unable to estimate the orientation of its rotation axis. In June 2023, at the initiative of the National Space Facilities Control and Test Center of State Space Agency of Ukraine (NSFCTC SSAU), a campaign was launched to obtain synchronous photometric observations of this RSO with the participation of several sensors. As a result, from June 2023 to July 1, 2024, 66 LCs of this spacecraft were obtained.

### 4. SENSORS

### 4.1 Ukraine

### 4.1.1 State Space Agency of Ukraine

For these observations the State Space Agency of Ukraine (SSAU) use two Optical-Electronic Optoelectronic Observation Stations (OEOS): OEOS-2 and OEOS-3 (Fig. 3). They are part of the National Space Facilities Control and Test Center (NSFCTC).



a)                                                                                    b)

Fig. 3. Optical sensors of SSAU: a) OEOS-2; b) OEOS-3.

The OEOS-2 is a high-aperture lens (f/1.0) mounted on a modified German direct drive mount located near Kyiv. The OEOS-3, located in western Ukraine. in the Zakarpatska region, consists of two lenses mounted on the same equatorial

mount: a wide field of view (WFoV) Hamilton lens and a narrow field of view (NFoV) Maksutov lens. In this campaign only WFoV lens of OEOS-3 was used. Both sensors are equipped with QHY-174M GPS CMOS cameras without filters and can track LEO objects. Their main characteristics are presented in Table 1. A more detailed description of both sensors can be found in [6] and [7].

Observations were carried out with an exposure from 20 to 100 ms. To process the received series of thousands of separate frames, ccd_phot software [8] was used. Before processing from the series, frames were removed, where the images of bright stars intersected with the image of an object or were from it at a distance smaller than 10 pixels.

Table 1: Main characteristics of OEOS -2 and OEOS -3

|  | OEOS -2 | OEOS -3 (WFoV only) |
|---|---|---|
| Aperture, cm | 30 | 35 |
| Focal length, m | 0.3 | 0.7 |
| Camera (chip) | CMOS with GPS | CMOS with GPS |
| FoV (deg$^2$) | 2.89 (130'x80') | 55'x35' |
| Mount | Equatorial with Direct Drive | Equatorial with Direct Drive |
| Slew rate, deg/s | Up to 10 | Up to 20 |
| Tracking | yes | yes |

#### 4.1.2. The Astronomical Observatory of Ivan Franko National University of Lviv

An optical telescope Celestron CPC 925 GPS (XLT) was used for observations non-cooperative space objects in the Astronomical Observatory of Ivan Franko National University of Lviv (AO LNU). It is Schmidt-Cassegrain telescope. The diameter is D=235 mm and focal length – F=2350 mm (Table 2). The telescope is installed on an alt-azimuth mount. (Fig. 4). The telescope is located in Lviv on the roof of the observatory.



Fig. 4. Celesron telescope of AO LNU.

The telescope is equipped with a a focus reducer GSO 0,5x, camera ZWO ASI174MM and filtr V. This sensor used ccd_phot [8] for processing of photometrical observations too.

Table 2: Main characteristics of Celestron

| Aperture, cm | 23.5 |
|---|---|
| Focal length, m | 2.35 |
| Camera (chip) | CMOS |
| FoV (deg$^2$) | 0.05 (16.3'x10.3') |
| Mount | Alt-Az |
| Slew rate, deg/s | Up to 5 |
| Tracking | yes |

### 4.1.3. Laboratory of Space Research of Uzhhorod National University

Laboratory of Space Research of Uzhhorod National University (LSR UzhNU) is located in western Ukraine, in the Zakarpatska region. It has two observational points – one in the city of Uzhhorod with AFU-75 telescope equipped with electrophotometer, and another is situated 15 km to the East from the city. Second observation point is equipped with 1 meter class telescope TPL-1M which was used as a mount for additional lens that was installed for photometry of LEO objects. This sensor is equipped with QHY-174M GPS CMOS camera with R filter. All characteristics of used telescopes are presented in Table 3 and on Fig. 5.



a)                                          b)

Fig. 5. Optical sensors of LSR UZhNU: a) TPL-1M; b) AFU-75.

Observations were carried out with an exposure value 500 or 1000 ms, processing of LCs was performed with ccd_phot software [8] developed in LSR UzhNU.

Table 3: Main characteristics of Laboratory of Space Research telescopes for LEO observation

|  | TPL-1M guide | AFU-75 |
|---|---|---|
| Aperture, cm | 12 | 10 |
| Focal length, m | 0.228 | 1 |
| Camera (chip) | CMOS with GPS | Photoelectronical multiplier (PhEM-79) |
| FoV (deg$^2$) | 2.5 (170'x106') | 5' (2 mm) |
| Mount | Alt-Az | Alt-Az |
| Slew rate, deg/s | Up to 3 | Up to 3 |
| Tracking | yes | yes |

### 4.1.4. Astronomical observatory of Odesa I.I.Mechnikov National University

Astronomical observatory of Odesa National University (AO ONU) is located in the south of Ukraine. It has a KT-50 telescope (Fig. 6) equipped with a TV CCD camera WAT-902H2 SUP for high-frequency photometry of low-orbit objects. Processing of photometric observations is done using their own software [9]. Characteristics of the telescope are given in Table 4.

Fig. 6. KT-50 telescope of AO ONU.

Table 4: Main characteristics of KT-50

| Aperture, cm | 50 |
|---|---|
| Focal length, m | 2.0 |
| Camera (chip) | TV-CCD |
| FoV (deg$^2$) | 0.03 (10.8' × 8.4') |
| Mount Type: | Alt-Az |
| Slew rate, deg/s | Up to 5 |
| Tracking | yes |

## 4.2 Italy

### 4.2.1 Sensors of S5Lab

Two telescopes S5Lab (Sapienza Space System and Space Surveillance) of the University of Rome "Sapienza" were used for observations, designed for positional and photometric observations of debris in different orbits: RESDOS (Remote Space Debris Observation System, Fig. 7a)) and SCUDO (Sapienza Coupled University Debris Observatory, fig. 7b)) [10]. The main characteristics of telescopes can be seen in the Table 5. RESDOS telescopes is located not far from Rome, and SCUDO - 80 km from Rome, in the observatory near Collepardo.



a)                                                                              b)

Fig.7. S5Lab telescopes: a) RESDOS; b) SCUDO.

Table 5: Main characteristics of S5Lab telescopes

| | RESDOS | | SCUDO | |
|---|---|---|---|---|
| | WFoV | NFoV | WFoV | NFoV |
| Aperture, cm | 15 | 40 | 15 | 25 |
| Focal length, m | 0.75 | 2.8 | 0.75 | 1.2 |
| Camera (chip) | sCMOS | CCD | sCMOS | sCMOS |
| FoV (deg$^2$) | 1.36 (1.27° x 1.07°) | 0.25 (30' x 30') | 1.36 (1.27° x 1.07°) | 1.145 (1.07° x 1.07°) |
| Mount | Equatorial | | Equatorial | |
| Slew rate, deg/s | yes | | yes | |

#### 4.2.2 BIRALES

BIRALES (BIstatic RAdar for LEo Survey) is a bistatic Italian radar of the UHF range (410-415 MHz) [11]. The transmitting part - Radio Frequency Transmitter (RFT) is a 7-m fully rotating mirror antenna (Fig. 8a)), which is located near the city of Cagliari, Sardinia. The maximum transmitting power is 10 kW. The width of the transmitting beam is 7.5°. The receiving part of BIRALES is located at the radio astronomy observatory of Medicine. It is part of the large UHF Northern Cross radio telescope. It consists of 16 fixed horizontally located parabolic antennas (Fig. 8b)) of the north-south part of the radio telescope. The total area of the BIRALES receiving part is 2,800 m$^2$, and the FoV is 6.6° x 2.2°.
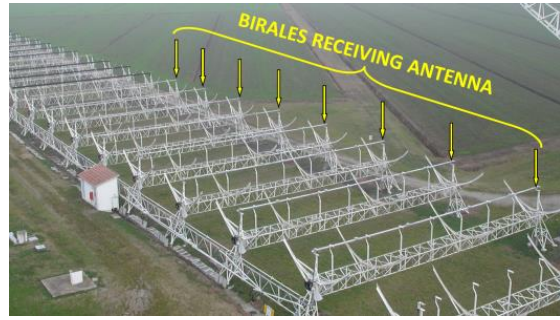


a)                                                                b)

Fig. 8. BIRALES: a) RFT; b) – receiving part.

#### 4.3 Switzerland

Observations were carried out by two telescopes of the Swiss Optical Station and the Geodynamic Observatory Zimmerwald of the Astronomical Institute of the University of Bern (AIUB) [12]: ZimLAT (Fig. 9a)) and ZimMAIN (Fig. 9b)). The main characteristics of both telescopes are shown in Table 6.

Table 6: Main characteristics of Zimmerwald observatory telescopes

| | ZimLAT | ZimMAIN |
|---|---|---|
| Aperture, cm | 100 | 80 |
| Focal length, m | 8 | 5.48 |
| Camera (chip) | CCD, sCMOS | CMOS |
| FoV (deg$^2$) | 0.19(26' x 26') | 0.15(23' x 23') |
| Mount | Alt-Az | Alt-Az |
| Slew rate, deg/s | Up to 30 | Up to 50 |
| Tracking | yes | yes |

|  |  |
|---|---|
| a) | б) |

Fig. 9. Telescopes of the Zimmerwald observatory participated in the observations: a) ZimLAT; b) ZimMAIN.

## 4.4 Japan

JAXA used the 35 cm Vixen SC355L telescope (Fig. 10) located at the Aerospace Center in Chofu, Tokyo for these observations. The main characteristics of the sensor are presented in Table 7
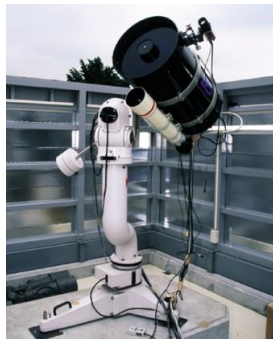


Fig. 10. Telescope Vixen SC355L in Chofu.

Table 7: Main characteristics of Vixen SC355L

| Aperture, cm | 35 |
|---|---|
| Focal length, m | 3.91 |
| Camera (chip) | CMOS |
| FoV (deg$^2$) | 0.01 (7.6'x6.1') |
| Mount | Three-axis |
| Slew rate, deg/s | Up to 5 |
| Tracking | yes |

## 4.5 Great Britain

The National Environmental Research Council Special Geodetic Facility (NERC SGF) main telescope, located near the village of Herstmonceux in East Essex [13], was used for the observations. This is a 50-cm Cassegrain telescope (Fig. 11, Table 8). Its main task is the laser location of space objects in frames of the International Laser Ranging Service (ILRS). Photometric observations are organized using a PMT detector.

Fig. 11. Main telescope of NERC SGF.

Table 8: Main characteristics of NERC SGF

| Aperture, cm | 50 |
|---|---|
| Focal length, m | - |
| Camera (chip) | PMT detector |
| FoV (deg$^2$) | - |
| Mount | Alt-Az |
| Slew rate, deg/s | Up to 5 |
| Tracking | yes |

**4.6 Latvia**

The LS-105 (Fig. 12) is the telescope of the Institute of Astronomy, University of Latvia Satellite Laser Ranging (SLR) station 1884 Riga, located at Kandavas St. 2, Riga, Latvia, in the University Botanical Garden service area. The main operation purpose of the system is to support the activities of the ILRS. It also has the capability to carry SLR observations in bistatic mode (passive) and photometric observations using the Andor iXon 888 EMCCD camera [14] installed on the Coudé LS-105 visual path. The camera has an adjustable field mask aperture that allows one to select only part of the sensor to increase frame rate.
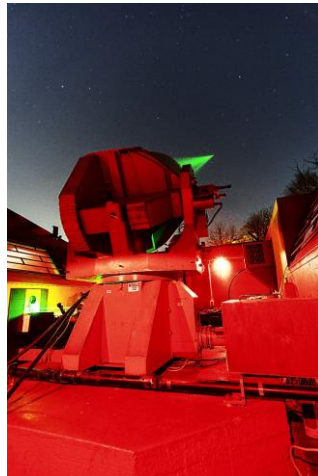

Fig. 12. Telescope LS-105.

The LS-105 is an Alt-Az Cassegrain system with a 1 m diameter main mirror and 25 cm diameter secondary mirror with an effective aperture of 96.8 cm (Table 9). The main optical system has a focal length of 11.6m. The LS-105 Coudé focus is shared by three different channels: a laser transmitter, a laser signal pulse receiver, and a visual

guidance channel. The Coudé focus channel sharing and switching is managed by two computer-controlled rotating mirrors using stepper motors.

Table 9: Main characteristics of LS-105 (photometry configuration)

|  | LS-105 |
| --- | --- |
| Aperture, cm | 100 (96.8 effective) |
| Focal length, m | 4 |
| Camera (chip) | EMCCD |
| FoV (deg$^2$) | 0.03 (11' x 11') |
| Mount | Alt-Az |
| Slew rate, deg/s | Up to 2.4 |
| Tracking | yes |

Photometric observations are currently carried out using standard sampling rates of 1 Hz, 2 Hz, and 10 Hz. The exposition times are always below 100ms, trying to use the lowest combination of EMCCD gain and exposition time, depending on the object's brightness.

For high-precision photometric rotation period determinations, the sampling trigger signal is synchronised from the Spectracom SecureSync 1200-033 GNSS steered Rb clock UTC 1PPS signal. The observations can be conducted without any filters or using the Krons-Cousins R &V filters.

This setup generated FITS files with a size up to 2 Gb with associated dark and flat frames using the same gain/exposition values. The observation time interval for a FITS file depends on the sampling rate, size of region of interest, and binning value. FITS files are processed using the OpenCV package.

## 5. PHOTOMETRICAL DATA ANALYSIS

### 5.1 Analysis of the LCs for 18340

Fig. 13 shows examples of LCs of 18340 RSO obtained at different sensors. During the specified campaign, the apparent rotation period of the 18340 smoothly increased from 55.6 sec to 142.7 sec. However, observations obtained in Zimmerwald (AIUB) on 12.07.2022 indicated a significantly reduced rotation period of the RSO. Subsequent observations at AIUB and in Ukraine confirmed the fact of further spinning of the spacecraft (Fig. 14, a). Therefore, the IADC Working Group 1 (WG1) supported the initiative of the SSAU to continue its photometric monitoring. As a result, it was discovered that the rotation of 18340 began to slow down again (Fig. 14, b). Note that the average growth rate of the rotation period in 2024 is only 0.02 seconds per day, which is almost 6.5 times slower compared to the growth rate of the rotation period in the interval August 2020 - July 2022.
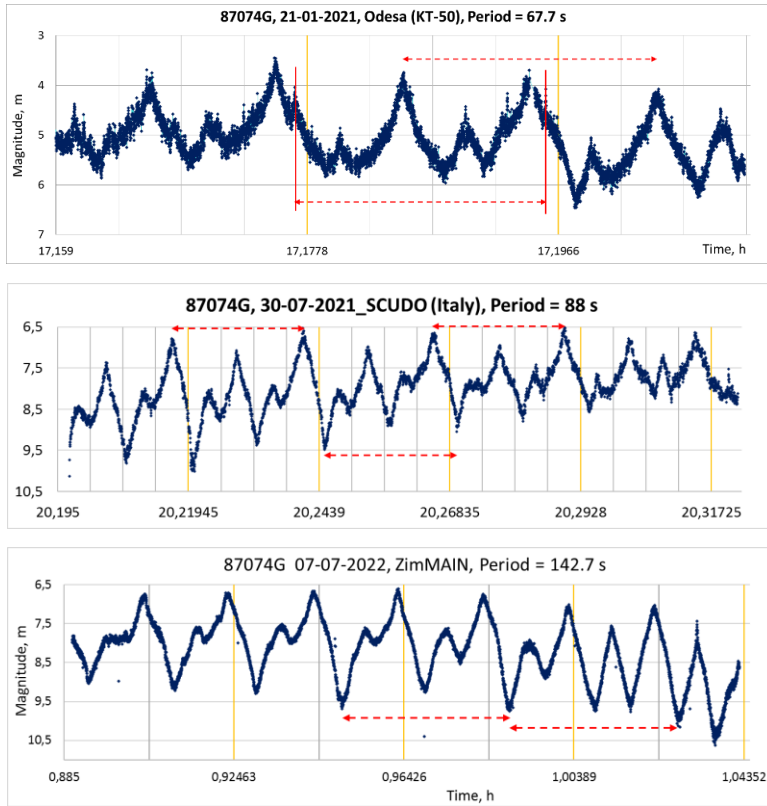
Fig. 13. Examples of LCs for 18340 obtained at different sensors.



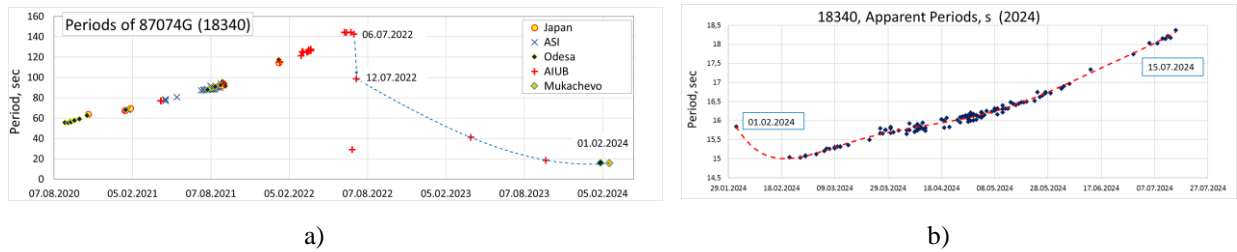a)                                                                    b)

Fig. 14. The apparent rotation period of the 18340: a) In 2020-2024. b) In 2024 mainly according to data from the NSFCTC SSAU.

We examined all obtained LCs for 18340 to identify similar fragments (photometric patterns). For the observation interval from April 14, 2021 to July 12, 2022, 94 different photometric patterns were selected. Examples of similar patterns from this list are shown in Fig. 15.
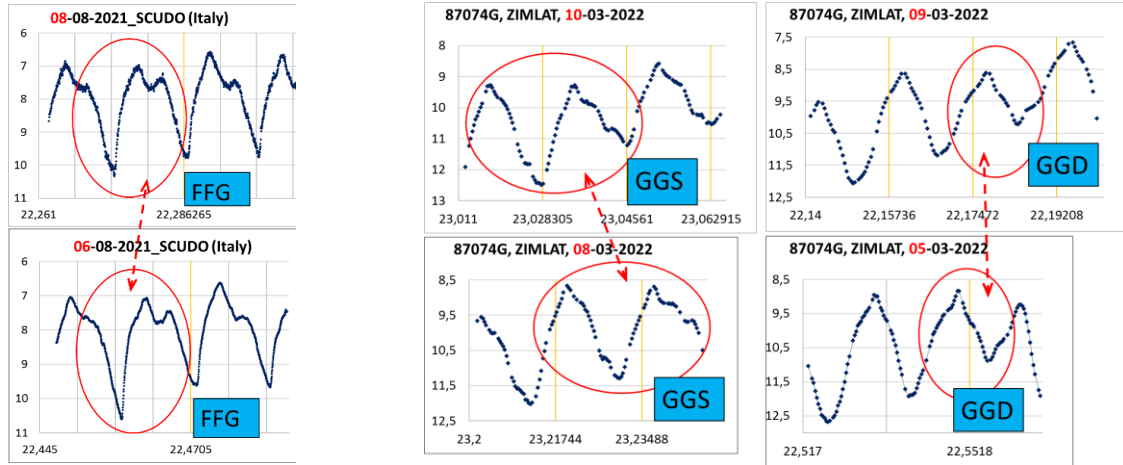
Fig. 15. Examples of patterns identified in the LCs of 18340. Three-letter abbreviations are conventional names of patterns.

Unfortunately, due to the rarity of observations in 2020-2022, as well as a rather long rotation period of the SC in this interval of observations (80 - 140 seconds), we were not able to reliably solve the obtained set of PAB-coordinates corresponding to the selected patterns. The reason is that the "best" solutions for method of least squares fall in the area of the location of the bisectors themselves in the celestial sphere.

During the 2024 observation campaign (from February 21 to June 5), the rotation period of 18340 varied in the range of 15 - 17 seconds. During this time, 111 LCs of 18340 were obtained (92 in NSFCTC, 8 in UKSA, 4 in JAXA, 3 in AO LNU, 3 in ASI and 1 in Latvia). The LCs have very different quality. From all this data, 251 patterns (27 different types) were identified. However, the possibility of obtaining a reliable solution for the rotation axis critically reduces the lack of good LCs obtained in close passages from different observatories. Basically, dense series of observations were obtained only at two sensors – in OEOS-2 and OEOS-3 (both in Ukraine). However, even among them, only eight are synchronous.

Having selected several pairs of similar patterns in the LCs obtained from different sensors synchronously or on adjacent orbits, we will find such an orientation of the RSO rotation axis, at which similar patterns refer to very close latitude values of the corresponding PABs. Fig. 16 shows the change in the latitude of the PAB vectors for the pole of the rotation axis RA = 10°, Decl = -66° and the corresponding photometric patterns obtained for the 18340 in two different passes on 27-02-2024 – in UKSA and in OEOS-3 (Mukachevo). We see how differently the latitude of the PABs changed at two sites with the adopted direction of the rotation axis (RA = 10°, Decl = -66°). Nevertheless, with this position of the rotation axis, similar patterns in different LCs appear at close values of the PAB latitude, and hence the latitude $\Phi_i$ in BFF.
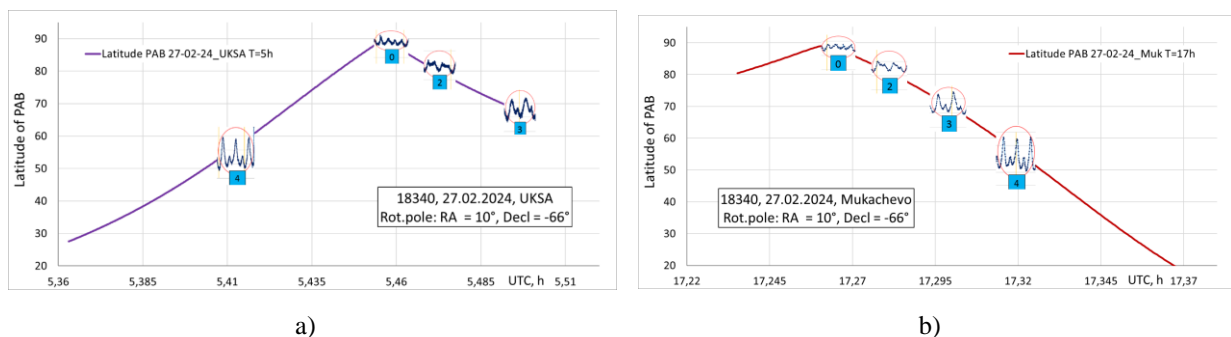


a)                                                        b)

Fig. 16. Change in PAB's latitude for the pole of the rotation axis RA = 10°, Decl = -66° and the corresponding photometric patterns (the type of pattern is indicated by its number), obtained during the passage of 18340 on 27-02-2024: a) UKSA; b) OEOS-3 Mukachevo.

On March 9, 2024 in AO LNU and on March 11 in OEOS-2 (Novosilki near Kyiv) very similar LCs of 18340 were obtained. This allowed us to identify several types of similar patterns on the two LCs. With the adopted direction of

the rotation axis (RA = 06°, Decl = -39°) at these two sites, the latitude of the PABs also changes in a similar way, and the corresponding similar patterns on the LCs appear at close values of the PAB latitude in the ARF (Fig. 17).



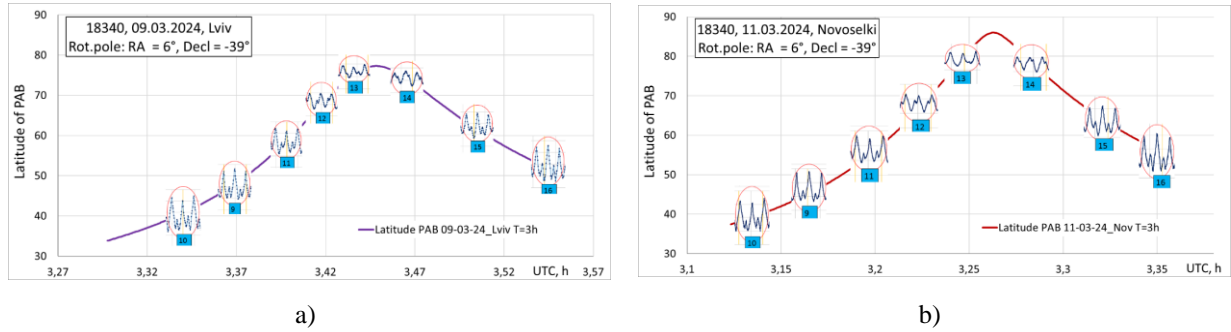a)                                                                                              b)

Fig. 17. Change in PAB's latitude for the pole of the rotation axis RA = 6°, Decl = -39° and the corresponding photometric patterns obtained during the passage of 18340: a) AO LNU on 09-03-2024; b) OEOS-2 (Novosilki) on 11-03-2024.

In these two examples of determining the direction of the axis of rotation, the amplitude of the used light curves changed significantly (this was visible in the images of the patterns accompanying the graphs of the change in the width of the PAB). Fig. 18a) shows the dependence of the amplitude of the light curves on the PAB latitude at the corresponding time points for six passes of 18340 in the interval March 9-11, 2024. With the inevitable spread of amplitude values (because they depend on several factors), we still see its monotonous decrease with increasing PAB latitude. For comparison, Fig. 18b) shows the dependence of the same amplitude on the phase angle. We see that this dependence is generally almost an order of magnitude less significant (slopes of 0.05 and 0.0066 magnitudes per degree, respectively).

This also indirectly confirms the correspondence of the obtained and real position of the axis of rotation of KA 18340 during this time interval.



a)                                                                                              b)
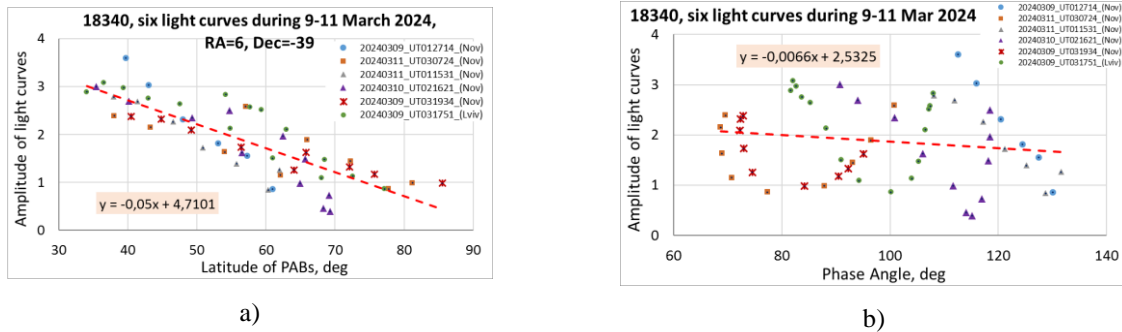
Fig. 18. Dependence of the LCs' amplitude on the latitude of PABs for six passes of the 18340 in the interval 09 – 11 March 2024 and the adopted direction of the rotation axis RA = 6°, Decl = -39° (a); Dependence of the LCs' amplitude on the phase angle (b).

## 6.2 Analysis of the LCs for 13552

Estimates of the apparent rotation period for the RSO 13552 are shown on Fig. 19. We see that the object is slowly decelerating at a constant speed and its rotation period is currently about 6.7 sec. This may indirectly indicate that the rotation of this fragment of the 13552 spacecraft occurs relative to a stable axis in the satellite's body.
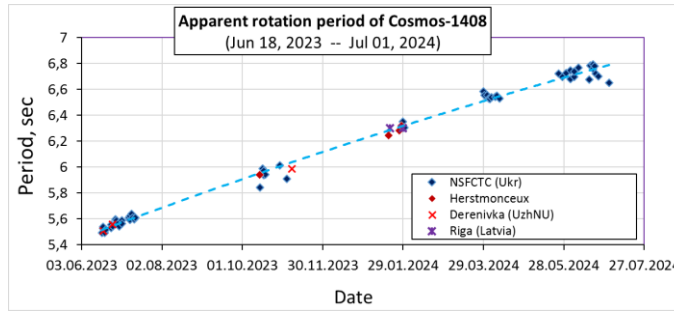
Fig. 19. Change in the apparent rotation period of 13552 in 2022-2024 based on photometric observations from several sensors.

Fig. 20 shows a fragment of the LC obtained on June 26, 2023 in OEOS-2. The LC is typical in structure for many other passages of this spacecraft and consists of a section with bright flares (amplitude 1.5$^m$-3$^m$), and a section with no bright flares. These two patterns are marked in the figure. Such a structure of the LCs allows us to find such an orientation of the spacecraft rotation axis when the latitude of all PABs corresponding to the interval of bright flares on the LCs obtained in neighboring passages falls into the general limited range of latitude values $\Phi_i = \beta\_PAB_i$ (see section 2).
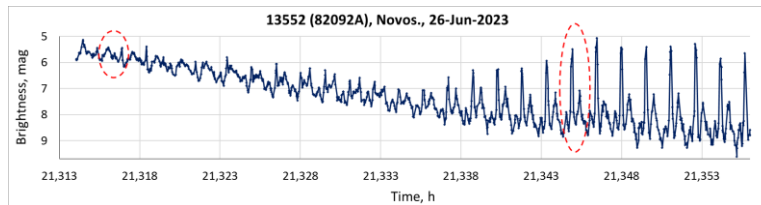


Fig. 20. A fragment of the LC of RSO 13552 obtained on June 26, 2023 in OEOS-2.

Fig. 21 shows the curves of the PABs latitude variation in seven passes of the RSO 13552 observed from two sensors (OEOS-2 and OEOS-3) in the interval of June 18-21, 2023. Fragments of these lines have different colors depending on the shape of the patterns in the corresponding sections of the LCs - the red dotted line corresponds to the presence of single bright specular flares (pattern 1), the purple dotted line corresponds to their absence (pattern 2). The green line corresponds to the section of the LC when the third type of pattern was observed, namely, four clearly visible specular flares during each period of the spacecraft rotation. For the rotation axis directed to the point with coordinates RA = 340°, Decl = + 12° in the inertial coordinate system, the PABs latitude in all fragments corresponding to the first type of pattern varies within -36° ÷ -51°. This may mean that in this latitude range in BFF there are normals to a smooth (quasi-mirror) section of the RSO surface reflects light towards the observer once per spacecraft revolution. In the latitude range "to the south" and "to the north" of this band there are no normals to such smooth sections. In the latitude range of +2 ÷ -11° a pattern was observed containing four small-amplitude brightness flares.
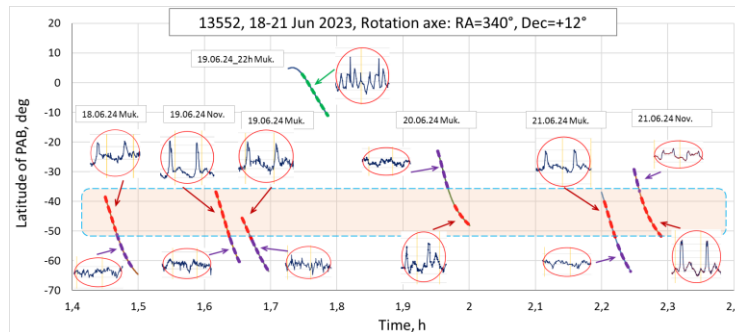


Fig. 21. PABs latitude variation curves in seven passes of the RSO 13552 observed from two sensors in the interval of June 18-21, 2023, with the adopted direction of the rotation axis (RA=340°, Decl=+12°). When the PAB latitude value falls within the highlighted zone, type 1 patterns are observed with a single bright flare during a full revolution of the RSO.

### 6.3 BIRALES observations of 13552

Unfortunately, data on the rotation period obtained by BIRALES do not coincide with the results of optical observations for the same time interval, although the tendency to increase the rotation period is observed in this case as well (Fig. 22). Perhaps it is necessary to analyze some other value than SNR, or to check whether all possible influencing factors are taken into account.
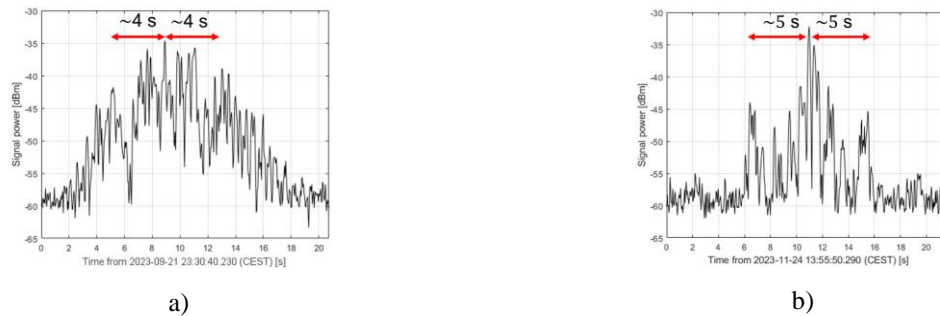


a)                                                                                    b)

Fig. 22. Estimates of the rotation period of KOSMOS-1408 obtained with the help of BIRALES in September (a) and November (b) 2023.

### 6. CONCLUSIONS

In this paper, we examined the structure of the LCs of two large space debris objects - 18340 and 13552. They were observed in different periods in 2020-2024. At the same time, the LCs obtained with the help of different hardware and software turned out to be relatively well matched with each other. Trends in the change in the rotation period of these RSO were determined. Based on the concept of a "photometric pattern" proposed in [3], we identified similar fragments on different LCs acquired over time intervals of about 1-3 days, which made it possible to made an estimate for the average direction of the RSO rotation axis in each of these intervals. As an example, this method is applied for the RSO 18340 based on two passes on February 27, 2024 (rotation axis coordinates RA = 10° ± 10°, Decl = -66° ± 10°) and on the LCs obtained on March 9 and 11, 2024 (rotation axis coordinates RA = 06° ± 10°, Decl = -39° ± 10°), and for the spacecraft 13552 based on six LCs obtained in the interval June 18-21, 2023 (rotation axis coordinates RA = 340° ± 10°, Decl = +12° ± 10°).

### REFERENCES

[1] L. Blacketer. Attitude Characterisation of Space Objects using Optical Light Curves. *A thesis for the degree of PhD. University of Southampton*, 2022.

[2] T. Hrobar et al. Attitude determination of cylindrical rocket bodies by using simultaneous bistatic photometric measurements. *AMOS Technical Conference Proceedings*, 2023.

[3] N. Koshkin et al. (2024). Determination of the spacecraft's spin axis orientation. Photometric patterns method. *Advances in Space Res.*, 2024. (https://doi.org/10.1016/j.asr.2024.08.038)

[4] N. Koshkin (ed.). (2021). Atlas of light curves of space objects. *Volume 6 (2019–2020)*, 2021. (*http://dspace.onu.edu.ua:8080/handle/123456789/32063*).

[5] D. Cerutti-Maori et al. Observation of Cosmos-1408 Debris Cloud with the Tracking and Imaging Radar System. *Proceedings of 2nd NEO and Debris Detection Conference*, 2023.

[6] O. Kozhukhov et al. Ukrainian Optical Sensors for Space Surveillance, *AMOS Technical Conference Proceedings*, 2020.

[7] O. Kozhukhov et al. New Two-Tubes Telescope for Observation of Near-Earth Space, *AMOS Technical Conference Proceedings*, 2022.

[8] V. Kudak, V. Perig. QHY-174M-GPS camera as the device for photometry of artificial satellites. *Artificial Satellites*, 57, 1: 47–57, 2022.

[9] L. Shakun et al. The observations of artificial satellites and space debris using KT-50 telescope in the Odessa university. *Odessa Astronomical Publications*, 29, 213-216. 2016. (http://oap.onu.edu.ua/article/view/85234/80990).

[10] F. Piergentili et al. LEO Object's Light-Curve Acquisition System and Their Inversion for Attitude Reconstruction. *Aerospace*, 8 (1), 4. 2021. (DOI: 10.3390/aerospace8010004).

[11] T. Pisanu et al. Upgrading the Italian BIRALES system to a pulse compression radar for space debris range measurements. *22nd International Microwave and Radar Conference (MIKON)*: 317-320, 2018. (DOI: 10.23919/MIKON.2018.8405212).

[12] E. Cordelli et al. Recent Developments at the Swiss Optical Ground Station and Geodynamics Observatory Zimmerwald. *Proceedings of 1$^{st}$ NEO and Debris Detection Conference*, 2019.

[13] http://sgf.rgo.ac.uk/index.html.

[14] https://andor.oxinst.com/assets/uploads/products/andor/documents/andor-ixon-ultra-emccd-specifications.pdf